DNA Melting in Small-Molecule−DNA-Hybrid Dimer Structures: Experimental Characterization and Coarse-Grained Molecular Dynamics Simulations

Tatiana R. Prytkova, Ibrahim Eryazici, Brian Stepp, Son-Binh Nguyen, and George C. Schatz*

Department of Chemistry, Northwestern University, Evanston, Illinois 60208-3113

Received: October 30, 2009; Revised Manuscript Received: January 6, 2010

When DNA hybridization is used to link together nanoparticles or molecules, the melting transition of the resulting DNA-linked material often is very sharp. In this paper, we study a particularly simple version of this class of material based on a small-molecule−DNA-hybrid (SMDH) structure that has three DNA strands per 1,3,5-tris(phenylethynyl)benzene core. By varying the concentration of the SMDHs, it is possible to produce either SMDH dimers or bulk aggregates, with the former having highly packed duplex DNA while the latter has an extended network. Melting measurements that we present show that the dimers exhibit sharp melting while the extended aggregates show broad melting. To interpret these results, we have performed coarse-grained molecular dynamics (CGMD) studies of the dimer melting and also of isolated duplex melting using CGMD potentials that have either implicit or explicit ions. Details of the melting simulation technology demonstrate that the simulations properly describe equilibrium transitions in isolated duplexes. The results show that the SMDH dimer has much sharper melting than the isolated duplex. Both implicit and explicit ion calculations show this effect, but the explicit ion results are sharper. An analytical model of the melting thermodynamics is developed which shows that the sharp melting is entropically driven and can be understood primarily in terms of the differences between the effective concentrations of the DNA strands for intracomplex hybridization events compared to intermolecular hybridization.

Introduction

Molecular self-assembly is the process whereby molecules adopt a well-defined structure without guidance or management from an outside source. Self-assembled molecular structures are ubiquitous in biology; for example, self-assembly results in the formation of cell membranes from lipids, the formation of double helical DNA through hydrogen bonding of nucleobases, and the arrangement of multiply folded proteins to form multisubunit complexes. Covalent bond formation is involved in the formation of key building blocks such as peptides and single stranded DNA; however, it is weak interactions, including hydrogen bonds, hydrophobic interactions, and electrostatics, that lead to the formation of fully functional tertiary structures. These principles can be used to produce complex multifunctional nanomaterials that can be used in biomimetics, medical diagnostics, therapeutics, photonic materials, and many other applications. It is important to learn how to describe and predict the self-assembly of these complex materials, but theory methods often have limited predictive capabilities due to the high dimensional space of configurations that is available when many structures self-organize.[1]

DNA is an example of a macromolecule which spans length scales from nanoscale (for short oligonucleotides) to macroscopic dimensions. In the last 10 years, there has been growing interest in the use of DNA to make complex structures. One version of this has involved using DNA to link together nanoparticles, viruses, and polymeric materials to form functional aggregates.[2] These materials have found use in sensing applications,[3] in part because they exhibit much narrower melting transitions (thermal dehybridization) than occur for the same duplexes in solution.[4] Upon the addition of DNA target complementary to the DNA primer strands that are attached to the gold nanoparticles (GNP−DNA), hybridization leads to the formation of large clusters or aggregates of nanoparticles.[5] Aggregate formation is conveniently observed in visible light as a color change from red to purple because of distant-dependent interactions associated with plasmon excitation in the gold particles.[3] It was found that, once the clusters are formed at a low temperature, the dissolution of clusters upon heating, monitored by the absorbance change at 520 nm (the surface plasmon band) or 260 nm (arising from hybridization of DNA plus nanoparticle absorption), is unusually sharp.[6] The well-defined character of the melting transition enables the detection of single-base mismatches between the probe and target DNA as a few degree shift in the melting temperature compared to the fully complementary melting curve.[7] Figure 1 schematically shows these results. The GNP−DNA system has an unusually high sensitivity for detection of the target DNA: target concentrations of tens of femtomoles can be detected calorimetrically, and even lower concentrations can be detected using a variety of amplification schemes.[8] While there has been much interest in the sensing properties of the GNP−DNA system, only recently it has been demonstrated that GNP−DNA aggregates can in some cases form crystalline (rather than amorphous) structures.[9] DNA-linked polymers have also been developed.[10−12] This leads to the possibility that DNA-tethered molecules might form the basis for a new class of structural chemistry elements for making functional materials.

Recently a new DNA-hybridization driven self-assembled system was developed that consists of a dimer of the small molecule 1,3,5-tris(phenylethynyl)benzene to which are attached three ssDNAs.[13] After hybridization at low concentration (0.38 μM), the dimer adopts a cage configuration which is schematically depicted in Figure 2. This SMDH (small-molecule−DNA-

* To whom correspondence should be addressed.

10.1021/jp910395k
Published on Web 02/05/2010

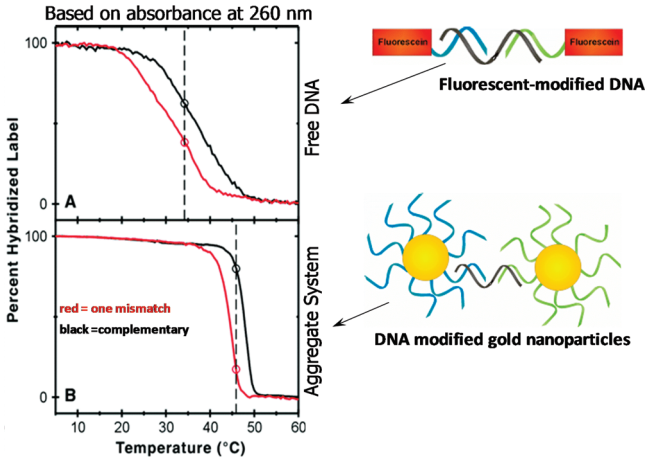

Figure 1. Melting curves associated with (A) duplex DNA and (B) DNA-modified gold nanoparticles (data adapted from ref 8).

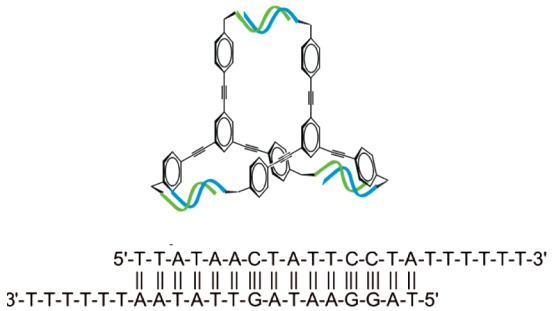

Figure 2. Caged shape dimer SMDH is formed from a tris(phenylethynyl)benzene core that serve as a linker for a three DNA molecules that are chemically attached to it with following sequence.

hybrid) dimer structure, which was originally reported by Nguyen and co-workers,[13] represents the simplest DNA-linked structure made to date that shows sharp melting, and unlike the aggregated materials described above, only two molecules are hybridized together in this structure. This means that in contrast to the infinite network of materials that have been prepared previously, the melting transition in this case cannot be modeled as a macroscopic (or even microscopic) phase transition. In addition, it was found that at high SMDH concentrations, hybridization leads to the formation of an extended network structure that does not show sharp melting.

The well-defined structure and relatively small size of the SMDH dimer provides an opportunity to use it as a test ground for investigations of the underlying physical mechanism for sharp melting transition found in DNA-linked structures. For the GNP−DNA and DNA-linked polymer aggregates, there has been significant interest in this issue,[7,14−20] and over the years two mechanisms have received alot of attention. First, the transition from a gel-like aggregate to a dilute phase is a phase transition and therefore perfectly sharp for an infinite system and still quite sharp for a finite system of sufficient size (as has been determined from direct simulation[19−21]). Second, if there are many DNAs that link together each nanoparticle, then there is the possibility that the DNAs can interact through their shared counterion clouds, leading to cooperative melting that would even apply to a dimer structure.[22,23] These two mechanisms can both operate for the DNA−DNA or polymer−DNA systems, so past theory work has developed approaches which combine the two. However for the SMDH dimer, we are in the unique position that the importance of just the shared ion-cloud mechanism can be tested. We can also determine if other contributions to cooperative melting might exist.

In this paper we present a combination of analytical theory, computational modeling, and new experimental results which are designed to establish the origin of sharp melting in the SMDH dimers. The theory refers to a simple thermodynamic model of dimer melting that uses local DNA concentrations to determine entropic contributions to the free energy change in each step of melting of the three DNAs. The computational modeling is done using a coarse-grained molecular dynamics approach in which the melting equilibrium is explicitly evaluated for the SMDH structures. The coarse-grained model reduces the number of atoms in DNA such that each nucleotide is represented by three beads and the bead−bead interactions average over atomic level details. This makes it possible to simulate the melting transition explicitly for sufficiently long time scales that equilibrium melting curves can be determined. By comparing results for the melting of duplex DNA in solution with those for the SMDH dimer, we show that the dimer structure has a much sharper transition whose properties are in qualitative agreement with new experimental data that we also present. In addition, we are able to use the simulations to elucidate the mechanism of sharp melting. The calculations show that the constrained structure of the SMDH dimer provides conditions in which most of the free energy release does not occur until the last stage of melting, i.e., breaking of the last duplex linking the molecules. This results in a cooperative mechanism, as melting of all the DNAs except the last duplex is entropically disfavored and requires a higher temperature than for duplex DNA. We show that this behavior is consistent with the analytical theory, and the theory suggests that constraints on the DNA motions lead to an effective DNA concentration for intracomplex dehybridization which is nearly constant for all steps in dehybridization except when the last DNA dehybridizes and the complex dissociates into two molecules. Counterion release also contributes to the free energies, and to sharpening of the melting curves, but the picture that emerges from this is more general than the simple shared ion-cloud mechanism described above.

Methods

A. Experiments. ***1. General Procedures, Materials, and Instrumentation.*** Synthesis of the DNA sequences was performed on an Expedite 8909 Nucleic Acid system. Unmodified DNA was purified on an Agilent 1100 HPLC equipped with a Varian Dynamax column (250 mm × 10.0 mm (L × I.D.), Microsorb 300−10 C18) using a gradient method beginning with 95:5 0.1 M TEAA:acetonitrile (TEAA = triethylammonium acetate) and increasing to 60:40 0.1 M TEAA:acetonitrile over 70 min, with a flow rate of 3 mL/min. Absorption spectra and melting analyses of DNA materials were recorded on a Varian Cary 300 Bio UV−vis spectrophotometer using a Starna quartz cell (path length = 10 mm). Nanopure water (18.2 MΩ cm resistivity) was obtained from a Millipore system (Milli-Q Biocel).[24]

2. Melting Experiments. Hybridization mixtures of unmodified DNA were formed by combining equimolar amounts of two cDNA species in PBS buffer, annealing the resulting mixture at 85 °C for 10 min, and allowing the solution to cool to room temperature over 3 h. Aggregates were denatured by heating the samples from 20 to 70 °C at a rate of 0.5 °C per minute while monitoring the UV absorbance at 260 nm at 0.25 °C intervals to determine the melting progress.

B. Coarse-Grained Molecular Dynamics Simulations. To simulate SMDH melting, we used a coarse-grained molecular dynamics (CGMD) model which is similar to one previously

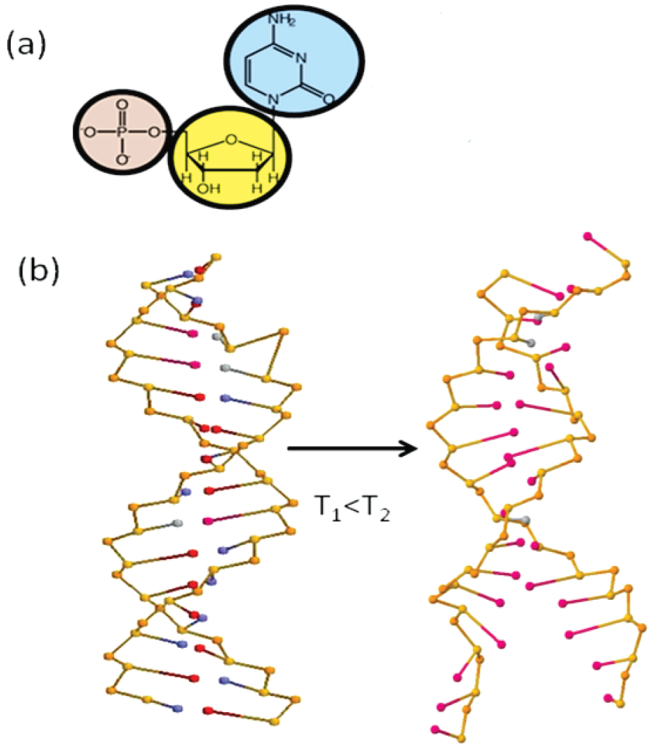

Figure 3. (a) Grouping of atoms for each interaction site of the coarse-grained model. (b) Snapshots of an intact and partially melted 15 bp model of DNA.

developed by Knotts et al[25] (and which follows up earlier work by Drukker and co-workers[26,27]). In this approach each nucleotide is represented by three interaction sites: phosphate, sugar, and base. The model (see Figure 3a) includes four types of bases that correspond to the four base types in DNA.

In contrast to the uncharged coarse-grained model of Drukker et al.[26] this model has charges of −1 on each phosphate so it can qualitatively reproduce the salt dependence of melting transitions. Our implementation of the model published by DePablo and co-workers[25,28] has some additional improvements concerning boundary conditions and the inclusion of explicit counterions. We included finite boundary conditions in our simulations, which is essential for simulating DNA melting under equilibrium conditions where both hybridization and dehybridization occur many times before meaningful statistics are obtained. This is impossible in molecular dynamics simulations without finite boundaries such as in ref 25 because after dehybridization the two strands of DNA will diffuse apart and the probability that the strands will eventually rehybridize is very small. To impose boundary conditions, we included a box-shaped repulsive potential around the molecule. The size of the boundary box in our simulations is 55 Å for free DNA and 120 Å for the SMDH dimer simulations. This size allows for several hybridization/dehybridization transitions to occur during the simulations while at the same time being large enough that the DNA strands can separate to the point of having negligible interactions. The concentration of DNAs in the box is higher than that used in the experiment, so melting is faster than it would be for simulations which use a box size that matches the experimental concentration. It is important to take this concentration difference into account in defining melting curves, as the boundaries significantly change the entropy release. We take this entropy change into account by calculating the entropy of dilution $\Delta S_{dil} = R \ln(C_{exp}/C_{box})$ where C_{exp} is the experimental concentration, 0.38 μM, and $C_{box} = 1/N_{AV}V_{box}$ where N_{AV} is Avogadro's number.[29]

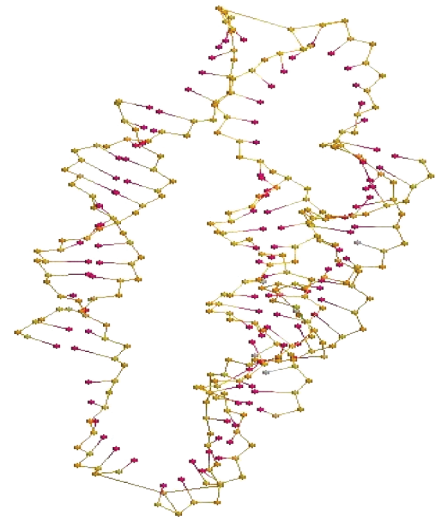

Figure 4. Coarse-grained model of the SMDH dimer.

To compare with the experimental melting curves, we calculate an entropy of dilution correction factor equal to $\Delta S/(\Delta S + \Delta S_{dil})$ where ΔS is the entropy of melting obtained from the theoretical melting curve by using a standard Van't Hoff procedure. Then we take this into account by multiplying the temperatures in the simulation by the correction factor. To generate melting temperatures that agree with experiment for free DNA, we built a free DNA molecule with the same sequence as in ref 24 and ran several simulations to identify the strength of hydrogen bonds needed in our ΔS_{dil} correction in order to match experiment. We found that the hydrogen bonds needed to be strengthened by a factor of 1.26 compared to that in the DePablo model to reproduce the experimental melting temperature with dilution included. Then we did simulations with the same hydrogen bond strength for the SMDH complex.

Another improvement on the Knotts et al.[25] model that we implemented is that we explicitly included Na^+ ions in the calculations, rather than using the implicit Debye−Huckel approximation scheme implemented in ref 25. This allows us to describe shared ion-cloud effects in the description of SMDH melting. In addition, the boundary box allows us to maintain a constant salt concentration with explicit ions, which would be impossible without boundary conditions.

One further complication was that the structure of the organic part of the SMDH complex needed to be defined separately from the DNA. To do this, we built an atomistic model of the SMDH dimer complex and then identified the equilibrium structure of the organic part to build a coarse-grained model of SMDH. The SMDH complex includes three parallel DNA molecules 15 bp in length connected by a DNA linker using a T6 sequence. All three linkers are connected to the organic molecule 1,3,5-tris(phenylethynyl)benzene, forming the cage shape molecule in Figure 4.

We created a simplified coarse-grained model of the organic linker molecule using only one coarse-grained atom that is connected to each T6 by a bond with length 11 Å. The force constant is 100 kcal/mol A^2, the angle force constant is 63 kcal/mol rad^2 with an equilibrium angle of 120°, and the mass is equal to the mass of the organic molecule. Figure 4 shows the resulting structure.

Using the coarse-grained model for the organic linker molecule (instead of an atomistic representation) allowed us to

run simulations with a longer time step of 10 fs. We ran 10 μs length simulations for free DNA and 20 μs length simulations for the SMDH complex. We used Langevin molecular dynamics for the simulations with explicit ions. To calculate melting curves, we ran simulations for a single molecule and calculated the average number of hydrogen bonds for this trajectory. Dividing this by the maximum number of hydrogen bonds gives the fraction of melted DNA. Note that this treatment assumes that the number of hydrogen bonds for a single duplex is equal to the average number of DNAs that are melted in an ensemble. This likely mimics what is actually measured, but it ignores processes such as end-fraying, whereby some bases may dehybridize without actually dissociating the duplex.

Theory and Simulation Results

A. Analytical Modeling. As a first step of the analysis, we will develop an analytical description of the melting equilibrium in free DNA and the SMDH complex based on the standard two-state model in which each DNA is either hybridized or dehybridized with no intermediate stages allowed. Some concepts in this derivation are related to earlier work by Licata and Tkachenko.[30]

If we consider the melting of free DNA, we can get an analytical expression for the fraction of ssDNA, $f(T)$, in terms of an equilibrium constant K which governs the reaction 2ssDNA $\rightleftarrows$ dsDNA. The equilibrium expression is given by (note that we represent all the equilibria in this section in terms of hybridization rather than dehybridization):

$$K = \frac{C(f(T) - 1)}{\left(\frac{1}{2}f(T)C\right)^2}$$

where C is total concentration of ssDNA upon complete dissociation. This equilibrium constant can also be expressed as:

$$K = e^{-(\Delta H - T\Delta S)/RT}$$

where ΔH and ΔS are the enthalpy and entropy of DNA melting.

By solving the equation above for $f(T)$, we generate an analytical expression for the melting curve as follows:

$$f(T) = \frac{2\sqrt{1 + KC} - 1}{KC}$$

From the experimental melting curve for duplex DNA having the same base-pair composition as in the SMDA, it can be estimated that $\Delta H = 107.7$ kcal/mol and $\Delta S = 374.1$ cal/(mol K). If we use these values as parameters, the resulting analytical melting curve in Figure 6 is obtained. Note that the melting temperature obtained from this analytical melting curve agrees reasonably well with the experimental melting temperature.

To determine an analytical expression for the SMDH melting curve, we consider intermediate states in the SMDH melting that are presented in Figure 5a. These include the intact SMDH dimer, the dimer with one DNA melted, the dimer with two DNAs melted, and two SMDH monomers in which all three DNAs are melted. If we denote the concentration of monomer containing only free DNA as [a], the concentration of monomer with complementary free DNA as [b], the concentration of the fully hybridized dimer as [ab$_3$], the concentration of the complex

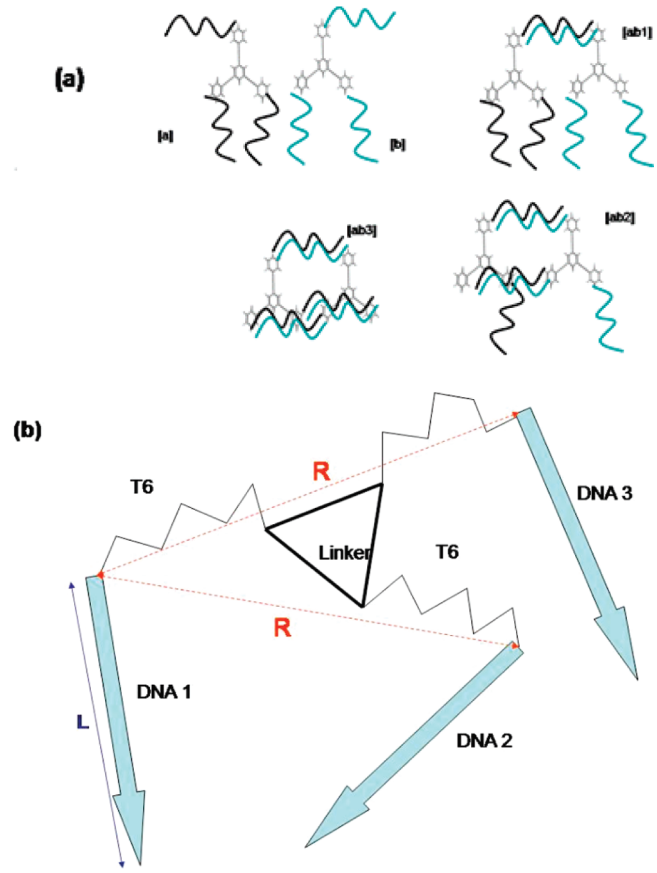

Figure 5. (a) Schematic of the SMDH complex, showing the four possible melting states. (b) Coordinate definitions used for the entropy calculation for the [ab$_1$] and [ab$_2$] states.

with one melted DNA as [ab$_1$], and the concentration of SMDH with two melted as [ab$_2$], then the total concentration of ssDNA, C_{total}, is

$$C_{\text{total}} = 3([a] + [b] + 2[ab_1] + 2[ab_2] + 2[ab_3]) \quad (1)$$

and the fraction of ssDNA observable in an experiment is

$$1 - f = \frac{2([ab_1] + 2[ab_2] + 3[ab_3])}{C_{\text{total}}} \quad (2)$$

To analyze this expression, we first consider the hybridization of [a] and [b] to give [ab$_1$]. The equilibrium constant expression for this species is given by

$$K_1 = \frac{[ab_1]}{9[a][b]} = e^{-(\Delta H - T\Delta S)/RT} \quad (3)$$

which assumes that the thermodynamic parameters that govern the hybridization of the one DNA are the same as those for free DNA. The coefficient 9 in the denominator reflects the probability of each DNA in one monomer to hybridize with each of three DNA strands from another monomer. This is included so that K_1 refers to each duplex within the dimer rather than to all duplexes. This makes K (for duplex DNA) and K_1 identical for the same temperature.

For the hybridization reaction going from $[ab_1]$ to $[ab_2]$, it is convenient to express the equilibrium for what nominally is a unimolecular reaction in terms of an expression similar to eq 3 for a bimolecular reaction using an effective concentration. This effective concentration arises because before hybridization of the second DNA strand, the nonhybridized part of the SMDH molecule cannot move freely and independently in solution but is constrained by an organic linker and the first hybridized DNA. We denote the bimolecular equilibrium constant for this reaction as K_2. By analogy with eq 3, we write:

$$K_2 = \frac{[ab_{eff1}]}{[a_{eff1}][b_{eff1}]} = e^{-(\Delta H - T\Delta S)/RT} \quad (4)$$

In this equation $[a_{eff1}] = [b_{eff1}]$ is the effective concentration for the SMDH complex which has one DNA hybridized, and $[ab_{eff1}]$ is the effective concentration for complexes which have one DNA hybridized and after reaction have two DNAs hybridized. Note that we are assuming that the effective concentrations are defined so that $K_2 = K_1$. In addition, we assume that the effective concentration ratio $[ab_{eff1}]/[b_{eff1}]$ is the same as the physical concentration ratio $[ab_2]/[ab_1]$. In other words, we have

$$\frac{[ab_2]}{[ab_1]} = \frac{[ab_{eff1}]}{[a_{eff1}]}$$

In this case, it is possible to write:

$$\frac{[ab_2]}{[ab_1]} = [a_{eff1}]e^{-(\Delta H - T\Delta S)/RT} \quad (5)$$

There are similar expressions which can be developed for the hybridization of the third DNA in the dimer. In this case we will use the effective concentration $[a_{eff2}] = [b_{eff2}]$ for the complex which has two DNA hybridized, and $[ab_{eff2}]$ for the complex which has two DNA hybridized and after reaction three DNA hybridized. Also, we require that the ratio of real concentrations be the same as the ratio of effective concentrations, i.e.,

$$\frac{[ab_3]}{[ab_2]} = \frac{[ab_{eff2}]}{[a_{eff2}]}$$

The equilibrium constant for this reaction, K_3, which we equate to K_1 and K_2, is given by:

$$K_3 = \frac{[ab_{eff2}]}{[a_{eff2}][b_{eff2}]} = e^{-(\Delta H - T\Delta S)/RT} \quad (6)$$

This leads us to:

$$\frac{[ab_3]}{[ab_2]} = [a_{eff2}]e^{-(\Delta H - T\Delta S)/RT} \quad (7)$$

If we assume that [a] = [b]. Then from eq 3

$$[ab_1] = 9[a]^2 e^{-(\Delta H - T\Delta S)/RT}$$

We will denote

$$p_0 = e^{(-\Delta H - T\Delta S)/RT}, \quad p_1 = \frac{[ab_2]}{[ab_1]}, \quad p_2 = \frac{[ab_3]}{[ab_2]}$$

so that the above equilibrium expressions become:

$$[ab_1] = 9p_0[a]^2$$

$$[ab_2] = p_1[ab_1]$$

$$[ab_3] = p_2[ab_2]$$

From expression (eq 1) for C_{total}, we can conclude that

$$C_{total} = 3\{2[a] + 2[ab_1](1 + p_1 + p_1p_2)\}$$

which can be rearranged to:

$$2[a] + 2p_0(1 + p_1 + p_1p_2)[a]^2 - \frac{1}{3}C_{total} = 0$$

The solution to this quadratic equation is:

$$[a] = \frac{-1 + \sqrt{1 + \frac{1}{3}AC_{total}}}{A} \quad (8)$$

where $A = 2p_0(1 + p_1 + p_1p_2)$. By using the equations

$$[ab_1] = p_0[a]^2 \quad (9)$$

$$[ab_2] = [ab_1][ab_{eff1}]e^{-(\Delta H - T\Delta S)/RT} \quad (10)$$

$$[ab_3] = [ab_2][ab_{eff2}]e^{-(\Delta H - T\Delta S)/RT} \quad (11)$$

and eqs 2 and 8, we can a plot melting curve for the SMDH aggregate. The slope of this melting curve will be determined by the $[ab_{eff1}]$ and $[ab_{eff2}]$ effective concentrations. These can be calculated using the structures of the complexes, as we now describe. Note that these effective concentrations determine the effective configurational entropy change during hybridization.

To estimate the effective concentrations we make the assumption that the effective concentration $[ab_{eff1}]$ of the second DNA in the complex after the first DNA is already hybridized is proportional to the effective volume that the second DNA can occupy. A simplified approach to estimate this volume involves considering the geometrical shape of the molecule as illustrated in Figure 5b. In this case the effective volume is estimated as the volume of sphere with radius R:

$$V_{eff1} = \frac{4}{3}\pi R^3$$

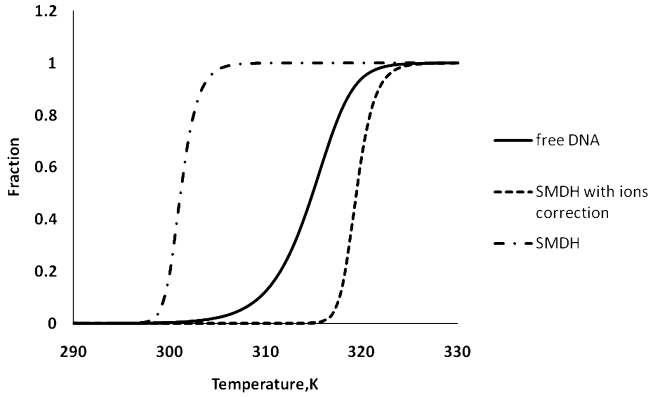

Figure 6. Melting curves from the analytical model.

If we assume that size of the linker size 16 Å and the length of single stranded T6 adjacent to linker 20 Å, we find $R = 56$ Å (see Figure 5b) and:

$$[\mathrm{ab}_{\mathrm{eff1}}] = \frac{1}{V_{\mathrm{eff1}}} = 2.27 \times 10^{-3}\ \mathrm{M/L}$$

If we assume that the effective concentration $[\mathrm{a}_{\mathrm{eff2}}]$ of the third DNA in the complex after the second is hybridized is proportional to the effective volume that the third DNA can cover, then from Figure 5b it can be seen that this volume is equal to the volume of a sphere with radius R.

This leads to:

$$[\mathrm{ab}_{\mathrm{eff2}}] = \frac{1}{V_{\mathrm{eff1}}} = 2.27 \times 10^{-3}\ \mathrm{M/L}$$

After substituting these estimated values of the effective concentrations, together with the earlier estimates for the thermodynamic parameters ΔH and ΔS into eqs 2 and 8−11, we obtain the melting curve presented in Figure 6. It can be seen from this figure that the model captures the main features of the sharp melting transition described in the experiment.

However, notice that the use of the free DNA value for ΔH leads to a much lower melting temperature, 301 K, than is observed in the experiment. This suggests that ΔH and/or ΔS for the SMDH complex need to be modified compared to the values for free DNA in order to obtain a melting temperature comparable to experiment. In the next section we show how it is possible to use molecular dynamics calculations to estimate ΔH and ΔS for the SMDH complex and for free DNA, and the results show that both contribute to changes in the melting temperatures. ΔH is calculated from the average potential energy of the melted and unmelted states. The results show that ΔH for melting the first, second, and third DNA in the SMDH dimer is increased by 6% compared with that for free DNA. Most likely the physical reason for this increase is because the electrostatic interactions associated with DNA strands that are in close proximity result in a higher concentration of counterions in the overlapping ion clouds[31] and thus more efficient screening of the repulsive interactions of the charged phosphates in the SMDH dimer. As a result, the unmelted state has lower potential energy while the melted state has higher potential energy and therefore larger ΔH. The larger ΔH leads to higher melting temperatures, but this does not explain all of the effect needed.

For ΔS, we only consider the entropic contribution to DNA melting resulting from condensation of ions around the DNA strands (as this contribution is not contained in the analytical model). This entropic contribution of the sodium ions is associated with the fact that the unmelted states of DNA have a larger fraction of condensed ions than the melted state of DNA. This effect is not contained in the model above, so factoring this contribution to melting also contributes to the effective melting temperature. In order to estimate this contribution, we calculated the average number of sodium ions located not farther than 7 Å from the charged phosphates of the DNA and SMDH for snapshots of molecular dynamics trajectories (described in the next section) in the unmelted and melted states. We have chosen this distance because it corresponds to the Manning theory radius from the surface of DNA for binding of monovalent cations.[32] In our case, where the counterions concentration is 150 mM, this distance is also close to the Debye length. With this definition, we were able to calculate the difference in the average number of condensed sodium atoms on the unmelted and melted states of free DNA and the SMDH. This difference corresponds to an increase in ΔS equal to 13.9 cal/(mol K). By including this counterion contribution to ΔH and ΔS, we generate a melting curve comparable to the experimental result (Figure 6, dashed curve).

We can use the analytical approach for studying DNA melting in the SMDH complex to understand the physical origin of cooperative behavior that sharpens the melting curve. From this analysis, we find that there is a large change in configurational entropy when two SMDH molecules hybridize to form a DNA duplex but only a relatively small change in ΔS for the next two hybridization steps. This provides the main source of cooperativity in the melting process; however, other effects, such as changes in the fraction of condensed counterions during these hybridization steps, also play a role.

For the present analysis, we made a simplified estimate of the configurational entropy using an effective concentration that is proportional to the volume covered by the rigid DNA strands tethered to the linker. We assumed that the configurational entropy is proportional to logarithm of the inverse effective concentration of DNA, and this leads to entropy estimates that realistically produce the expected sharpening of the melting transition. In reality the DNA strands in the SMDH dimer have many complicated rotational and vibrational degrees of freedom that contribute to the entropy but are not included in our model. This effect is partially taken into account by using ΔS from the experiment as a parameter for parametrizing the analytical melting curves for duplex DNA; however, it is clear that this is a crude treatment, and therefore that more detailed simulations are needed to clarify the important physical factors involved.

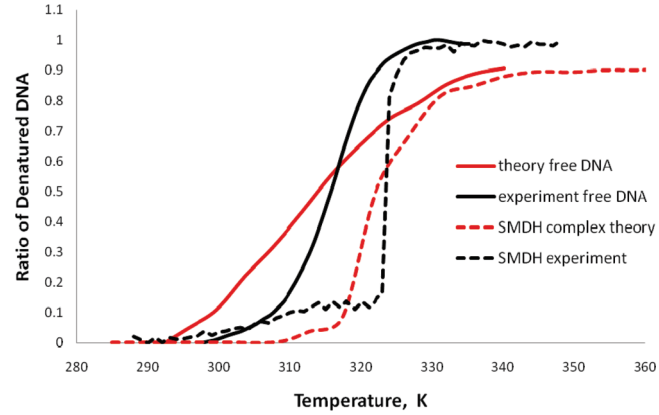

Figure 7. Theoretical and experimental melting curves for free DNA and the SMDH dimer, based on the explicit ion model.

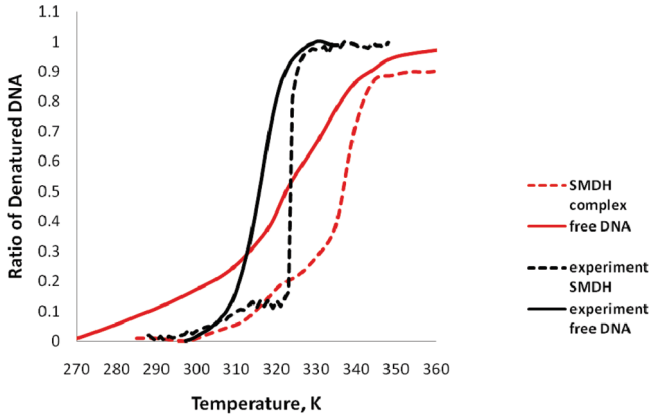

Figure 8. Theoretical and experimental melting curves for free DNA and the SMDH complex with an implicit Debye−Huckel model for the ions.

B. Coarse-Grained Modeling. As a second step in our analysis, we use a more sophisticated model based on the coarse-grained molecular dynamics method described earlier to simulate the SMDH melting transition. Figure 7 depicts melting curves obtained from the CGMD calculations, both for free DNA and the SMDH complex using an explicit representation of the counterions and an assumed salt concentration of 150 mM. The results are compared with experimental melting curves, and we note that qualitative agreement is found. The calculated melting temperature for free DNA is 313 K, and the melting temperature for the SMDH complex is 322 K. The experimental melting temperature is 313 K for free DNA and 323 K for the SMDH complex. We also see a sharpened melting transition for the SMDH complex that is similar to experiment. The sharpness of the melting curves reflects the higher ΔH for melting of the SMDH complex compared to the uncooperative melting of three duplex DNAs. This is connected to our earlier statement about the 6% increase in ΔH for the SMDH complex compared to three duplex DNAs, but there are entropic contributions as well which lead to a higher melting temperatures. Unfortunately it is difficult to use melting curve results to provide a more quantitative comparison of theory and experiment. Note also that the high temperature limit of the theoretical melting curves goes more slowly to unity than in the experiment. This is a limitation of the small volume used in the simulation, as this allows some hybridization to occur even when the DNAs are melted because of random encounters.

Figure 8 presents theoretical melting curves calculated for free DNA and the SMDH complex using an implicit Debye−Huckel representation of the salt, along with the same experimental data as in Figure 7. The calculated melting temperature for free DNA is 322 K, and the melting temperature for the SMDH dimer is 335 K. The melting transition for the SMDH complex is sharper than for free DNA for melting fractions greater than 0.3. The results in Figure 8 are similar to those in Figure 7, but the SMDH curve in Figure 7 is a little sharper.

To connect the mechanism for melting to our earlier analytical analysis, we have calculated entropy differences associated with the four possible stages of melting of the SMDH complex that were defined in Figure 5a. Ideally this analysis should be based on the SMDH simulations just described; however, this turns out to be difficult to do, as the SMDH dimer has a low probability for being in intermediate states at temperatures close to the melting temperature. To overcome this problem for the fully hybridized dimer, we ran simulations with the hydrogen bond strength taken to be 20% higher than normal, as this keeps the SMDH dimer hybridized. To create a SMDH dimer in a partially melted intermediate state, we mutated one or more selected DNA strands in this model to make them noncomplementary. Thus, if one strand is mutated, the SMDH dimer will, at the melting temperature, most of the time be in a state with one DNA melted. With this approach and assuming that the entropy change is not dependent on this increased hybridization enthalpy, we can easily evaluate the entropy differences between

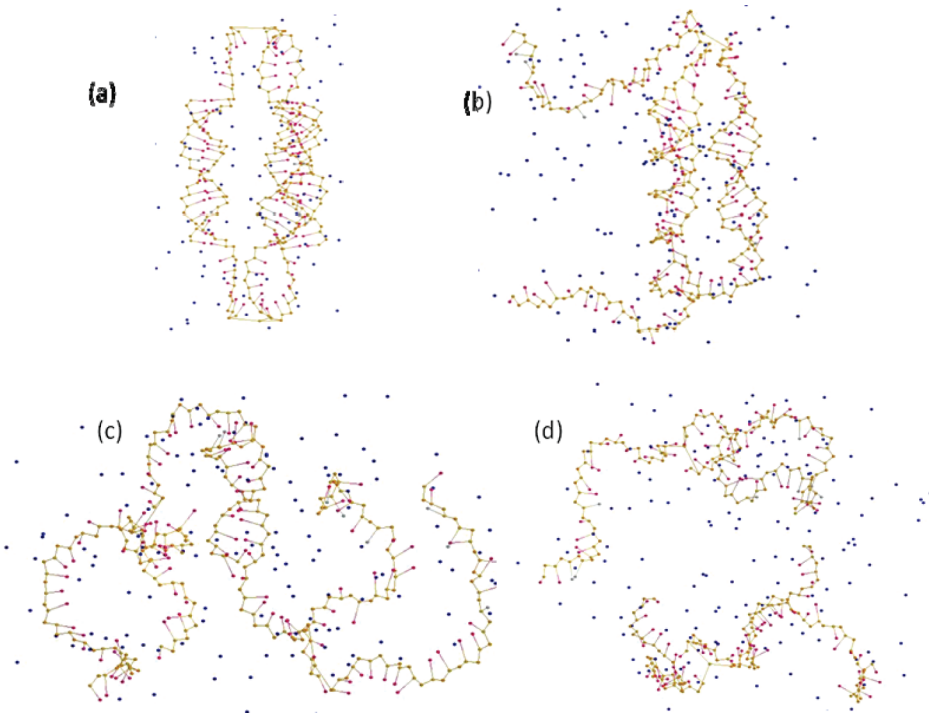

Figure 9. Snapshots from simulations of melting stages of the SMDH complex. (a) State 1: SMDH dimer with three hybridized DNAs. (b) State 2: SMDH with one DNA melted and two intact. (c) State 3: two DNAs melted, one intact. (d) State 4: all three DNAs melted.

TABLE 1: Entropy Differences Associated with the Four Melting Stages of the SMDH Cluster

entropy difference between states	ΔS, K/mol K
state 1 − state 2, ΔS_{12}	370.7
state 2 − state 3, ΔS_{23}	373.1
state 3 − state 4, ΔS_{34}	6762.4

TABLE 2: Entropy Difference between Duplex and Melted DNA

states of DNA	ΔS, K/mol K
intact − melted, $\Delta S_{\text{free DNA}}$	862.8

hybridized and melted states. Figure 9 depicts snapshots from these simulations.

We used the quasiharmonic method[33] to estimate the relative difference in configurational entropy for the four melting stages. From an average of the potential energy over the molecular dynamics trajectory, we also estimated ΔH. The results of the simulations are summarized in Table 1. For completeness, we ran similar types of simulations for duplex and free DNA. The resulting entropy change is presented in Table 2. Table 1 shows that most of the entropy increase is in the last stage of melting. Indeed ΔS_{34} is a factor of 20 higher than for the first two stages, ΔS_{12} and ΔS_{23}. In addition, note that ΔS_{12} and ΔS_{23} are smaller than $\Delta S_{\text{free DNA}}$ while ΔS_{34} is larger than $\Delta S_{\text{free DNA}}$. This means that the entropic driving force for the first two melting steps is less than in the melting of free DNA while that for the last step is larger. In contrast, the corresponding enthalpy changes, ΔH_{12}, ΔH_{23}, and ΔH_{34}, are approximately the same. As a result, it is easy to see that at the melting temperature T_{free} of free DNA, $\Delta G_{12} = \Delta H_{12} - T_{\text{free}}\Delta S_{12}$ and $\Delta G_{23} = \Delta H_{23} - T_{\text{free}}\Delta S_{23}$ will be positive while $\Delta G_{34} = \Delta H_{34} - T_{\text{free}}\Delta S_{34}$ will be negative. Therefore, in order for the first two stages of melting to occur, the melting temperature of the dimer must be larger than T_{free}, but when the temperature is raised to this point, the second and third stages of melting will also occur spontaneously as soon as the first step is completed. This means that the melting is cooperative.

While the results in Table 1 give us the correct trends, it is not possible to quantify further, as we used artificially perturbed states to determine the entropy changes for each stage of melting, and we have neglected changes in enthalpy compared to the simulation results in Figure 8. However, the important point of this analysis is that there is a strong entropic driving force for cooperative behavior.

Conclusions

This manuscript has presented a comprehensive analysis of the narrowed melting transitions associated with the SMDH dimer using a combination of experimental melting curves, analytical modeling, and simulations. Included in this analysis was the presentation of a new coarse-grained DNA model which includes explicit ions. In addition, we have presented a simulation technology for calculating melting temperatures using a finite box and for correcting the resulting melting curve for differences between the simulation and actual DNA concentrations.

The results of our simulations and analysis show (qualitatively) that the narrow melting transitions arise from entropic effects which mostly can be correlated to the effective concentration of DNA in the SMDH dimers. This result agrees with the earlier models by Licata and Tkachenko, but here we have used simulation to confirm the assumptions in the model. The counterions do contribute to the sharp melting, but larger effects arise from effective concentration effects. Clearly, an important project for the future will be to examine how the effective concentration varies for other DNA-linker structures, including the role of DNA density and linker structure. For DNA-linked gold nanoparticle structures, nanoparticle size and DNA density are all known to play an important role, but the correlation of these results with sharpness of melting has not been explained. The present analysis gives us the tools needed to do this.

Acknowledgment. This research was supported by National Science Foundation (grant CHE-0843832), by the NSEC Center at Northwestern (NSF grant EEC-0647560), and by the Northwestern Center for Cancer Nanobiotechnology Excellence (1 U54 CA119341-01).

References and Notes

(1) McCullagh, M.; Prytkova, T.; Tonzani, S.; Winter, N. D.; Schatz, G. C. *J. Phys. Chem. B* **2008**, *112*, 10388.
(2) Mirkin, C. A.; Letsinger, R. L.; Mucic, R. C.; Storhoff, J. J. *Nature* **1996**, *382*, 607.
(3) Storhoff, J. J.; Elghanian, R.; Mucic, R. C.; Mirkin, C. A.; Letsinger, R. L. *J. Am. Chem. Soc.* **1998**, *120*, 1959.
(4) Jin, R.; Wu, G.; Li, Z.; Mirkin, C. A.; Schatz, G. C. *J. Am. Chem. Soc.* **2003**, *125*, 1643.
(5) Storhoff, J. J.; Mirkin, C. A. *Chem. Rev.* **1999**, *99*, 1849.
(6) Storhoff, J. J.; Lazarides, A. A.; Mucic, R. C.; Mirkin, C. A.; Letsinger, R. L.; Schatz, G. C. *J. Am. Chem. Soc.* **2000**, *122*, 4640.
(7) Jin, R. C.; Wu, G. S.; Li, Z.; Mirkin, C. A.; Schatz, G. C. *J. Am. Chem. Soc.* **2003**, *125*, 1643.
(8) Taton, T. A.; Mirkin, C. A.; Letsinger, R. L. *Science* **2000**, *289*, 1757.
(9) Park, S. Y.; Lytton-Jean, A. K. R.; Lee, B.; Weigand, S.; Schatz, G. C.; Mirkin, C. A. *Nature* **2008**, *451*, 553.
(10) Gibbs-Davis, J. M.; Schatz, G. C.; Nguyen, S. T. *J. Am. Chem. Soc.* **2007**, *129*, 15535.
(11) Kudlay, A.; Gibbs, J. M.; Schatz, G. C.; Nguyen, S. T.; De la Cruz, M. O. *J. Phys. Chem. B* **2007**, *111*, 1610.
(12) Lytton-Jean, A. K. R.; Gibbs-Davis, J. M.; Long, H.; Schatz, G. C.; Mirkin, C. A.; Nguyen, S. T. *Adv. Mater. (Weinheim, Ger.)* **2009**, *21*, 706.
(13) Stepp, B. R.; Gibbs-Davis, J. M.; Koh, D. L. F.; Nguyen, S. T. *J. Am. Chem. Soc.* **2008**, *130*, 9628.
(14) Long, H.; Schatz, G. C. *Mater. Res. Soc. Symp. Proc.* **2003**, *735*, 143.
(15) Park, S. Y.; Stroud, D. *Phys. Rev. B* **2003**, *68*, 224201/1.
(16) Gibbs-Davis, J. M.; Schatz, G. C.; Nguyen, S. T. *J. Am. Chem. Soc.* **2007**, *129*, 15535.
(17) Kudlay, A.; Gibbs, J. M.; Schatz, G. C.; Nguyen, S. T.; De la Cruz, M. O. *J. Phys. Chem. B* **2007**, *111*, 1610.
(18) Park, S. Y.; Gibbs-Davis, J. M.; Nguyen, S. T.; Schatz, G. C. *J. Phys. Chem. B* **2007**, *111*, 8785.
(19) Lukatsky, D. B.; Frenkel, D. *Phys. Rev. Lett.* **2004**, *92*, 068302/1.
(20) Lukatsky, D. B.; Frenkel, D. *J. Chem. Phys.* **2005**, *122*, 214904/1.
(21) Park, S. Y.; Stroud, D. *Phys. Rev. B* **2003**, *67*, 212202.
(22) Jin, R.; Wu, G.; Li, Z.; Mirkin, C. A.; Schatz, G. C. *J. Am. Chem. Soc.* **2003**, *125*, 1643.
(23) Long, H.; Kudlay, A.; Schatz, G. C. *J. Phys. Chem. B* **2006**, *110*, 2918.
(24) Stepp, B. R.; Gibbs-Davis, J. M.; Koh, D. L. F.; Nguyen, S. T. *J. Am. Chem. Soc.* **2008**, *130*, 9628.
(25) Knotts, T. A.; Rathore, N.; Schwartz, D. C.; de Pablo, J. J. *J. Chem. Phys.* **2007**, 126.
(26) Drukker, K.; Schatz, G. C. *J. Phys. Chem. B* **2000**, *104*, 6108.
(27) Drukker, K.; Wu, G.; Schatz, G. C. *J. Chem. Phys.* **2001**, *114*, 579.
(28) Sambriski, E. J.; Schwartz, D. C.; de Pablo, J. J. *Proc. Natl. Acad. Sci. U.S.A.* **2009**, *106*, 18125.
(29) Ouldridge, T. E.; Johnston, I. G.; Louis, A. A.; Doye, J. P. K. *J. Chem. Phys.* **2009**, 130.
(30) Licata, N. A.; Tkachenko, A. V. *Phys. Rev. E* **2006**, *74*, 8.
(31) Long, H.; Kudlay, A.; Schatz, G. C. *J. Phys. Chem. B* **2006**, *110*, 2918.
(32) Wilson, R. W.; Rau, D. C.; Bloomfield, V. A. *Biophys. J.* **1980**, *30*, 317.
(33) Karplus, M.; Kushick, J. N. *Macromolecules* **1981**, *14*, 325.

JP910395K